IEEE Access
Multidisciplinary ⋮ Rapid Review ⋮ Open Access Journal

Received 2 August 2022, accepted 16 August 2022, date of publication 19 August 2022, date of current version 29 August 2022.

Digital Object Identifier 10.1109/ACCESS.2022.3200340

RESEARCH ARTICLE

Differential-Fed, Dual-Aperture Based, Quasi-End-Fire 5G mmWave Antenna-in-Package Design

M. IDREES MAGRAY[1], (Student Member, IEEE), SAOU-WEN SU[1], (Senior Member, IEEE), AND JENN-HWAN TARNG[2], (Senior Member, IEEE)

[1]Antenna Design Department, Advanced EM and Wireless Communication Research and Development Center, ASUSTek Computer Inc., Taipei 11259, Taiwan
[2]College of Electrical and Computer Engineering, Institute of Communication Engineering, National Yang Ming Chiao Tung University, Hsinchu 30010, Taiwan

Corresponding author: M. Idrees Magray (Idrees_Magray@asus.com)

This work was supported by the "Qualcomm Taiwan Research Program, 2020 [National Chiao Tung University/National Yang Ming Chiao Tung University (NCTU/NYCU)]" under Grant NAT435535 SOW.

ABSTRACT A low-profile, wideband antenna-in-package (AiP) design is proposed for 5G mmWave mobile applications. The aperture-coupled feeding incorporated with the microstrip feed line through the slots in the ground is used to excite the patch antenna. Firstly, a thin quarter-wave shorted patch antenna (QW-SPA) with the dominant $TM^{z}_{1/2,0,0}$ mode is realized. To broaden the operating band, the QW-SPA is extended along its resonant length so that the $TM^{z}_{1,0,0}$ mode can also be excited. The offset introduced into the two slots together with the additional shorting via wall are applied to enhance the beam tilt toward the end-fire direction. The proposed single-patch design shows a wide fractional bandwidth, covering the 5G mmWave band n257 (26.5–29.5 GHz). Furthermore, to increase more beam tilt, the differential-fed, two-patch sub-array formed by two QW-SPAs spaced a half-wavelength at 28 GHz apart is also presented. Compared with the single-patch design, the beam-tilt enhancement of around 10–27 degrees is obtained over the desired frequency band with the peak gain of around 8.2 dBi for the sub-array AiP design.

INDEX TERMS Patch antennas, antenna-in-package (AiP), fifth generation (5G) antennas, mmWave, beam tilt, thin quasi-end-fire antennas, aperture-coupled feed, differential feed.

I. INTRODUCTION

The advancement of the fifth generation (5G) communication for high-speed internet has attracted a lot of attention of researchers across the academia and industry to design and develop future transceivers in millimeter-wave (mmWave) frequency range. The candidate frequency bands include the new radio (NR) bands n257 (26.5–29.5 GHz) and n260 (37–40 GHz), which are centered respectively at 28 and 39 GHz and each with a bandwidth of 3 GHz [1].

Unlike the discrete antenna designs, the antenna-in-package (AiP) has become the standard packaging technology for mmWave applications, for example, 5G smartphones [2], 60 GHz radios [3], 94-GHz radar applications [4], etc. The AiP simplifies a few challenges at mmWave frequencies, for example, easier integration of the antennas with RF circuitry. On the other hand, the sub-6 GHz technology uses the power amplifiers, switches, filters, and discrete antennas separately. This leads to large space as the matching circuits between components are usually required to avoid the reflection. The insertion loss is also high because the connectors consume extra losses. These scenarios become different at mmWave frequencies because the components can be integrated as a package, called system-in-package (SiP). In the integration process, the AiP is regarded as one of the critical components, in which the antennas are designed on the multi-layered substrate. The AiP is mainly realized on the low temperature co-fired ceramic (LTCC) substrate, multi-layered organic substrates, silicon substrates, and multi-layered PCBs.

In addition, the end-fire antennas are preferred for 5G mmWave mobile applications due to the desired

The associate editor coordinating the review of this manuscript and approving it for publication was Giorgio Montisci.

line-of-sight communication and wide angular beam coverage [5]. For the implementation of the AiP design, it has recently become a standard to use a full-metal ground plane that can shield any deterioration in antenna characteristics caused by an integrated circuit (IC) beneath the antenna [6], [7], [8]. However, the full-metal ground can cause a decrease in total effective radiating volume, thereby reducing antenna bandwidth. Also, the modern 5G devices possess low form factor and therefore, the antenna thickness need to be compromised so that the antenna can be easily accommodated inside the 5G device. In this scenario, it is very difficult to design a thin substrate-based, end-fire antenna with a full-metal ground and at the same time, obtain a wide bandwidth and stable radiation patterns.

Several 5G mmWave AiP designs have been reported in the literature. For example in [5], the LTCC multi-layered, substrate-based planar folded slot antenna is introduced. Although the antenna carries the full-metal ground plane, the narrow impedance bandwidth and the unwanted beam tilt of 20–25 degrees (observed from the end-fire direction) in the E-plane are obtained. Also, the height of the antenna is 0.11-λ_0 at 38 GHz, which is too large to be implemented in modern mobile devices. A dual-polarized LTCC 18-layered end-fire antenna array is presented in [9]. The antenna can cover the entire n257 frequency band without any beam tilt. This design also lacks the full-metal ground/shielding plane and possesses a large thickness of 0.12-λ_0 at 28 GHz. In addition, various end-fire antenna designs have been proposed for 5G mmWave applications [10], [11], [12]. These antennas simply possess a large thickness and only partial shielding plane that might not be suitable for reliable 5G communication.

In this paper, we propose a thin and wideband differential-fed sub-array AiP design with full-metal ground plane. A thin substrate stack-up of thickness 0.5 mm (~0.05-λ_0 at 28 GHz) only is used for the realization of the proposed design. The objective for the proposed antenna configuration is to steer the radiation beam from broadside to end-fire direction with high gain. For achieving the same, a shorted single-patch radiator fed by a microstrip feed line through the two slots in the ground plane is first introduced. A wide impedance bandwidth of 14.3% is obtained due to the excitation of the $TM^z_{1/2,0,0}$ and $TM^z_{1,0,0}$ modes. The beam tilt of around 35° at 28 GHz is also obtained that is later enhanced by the introduction of the differential-fed two-patch sub-array, in which the beam tilt of around 45° at 28 GHz can be achieved. The beam tilt is attributed to the usage of the shorting via walls, the offset of dual apertures in the ground plane and differential feeding. The large beam tilt also produces high gain in the end-fire direction. The peak gain of around 8.2 dBi is obtained for the quasi-end-fire, sub-array AiP design.

The article is organized as follows. Section II describes the evolution of the single-patch AiP design and its working principle with the simulated and measured results discussed. Section III presents the differential-fed, two-patch sub-array formed by using the single-patch design proposed in Section II. Finally, Section IV summarizes the whole work and concludes the paper.

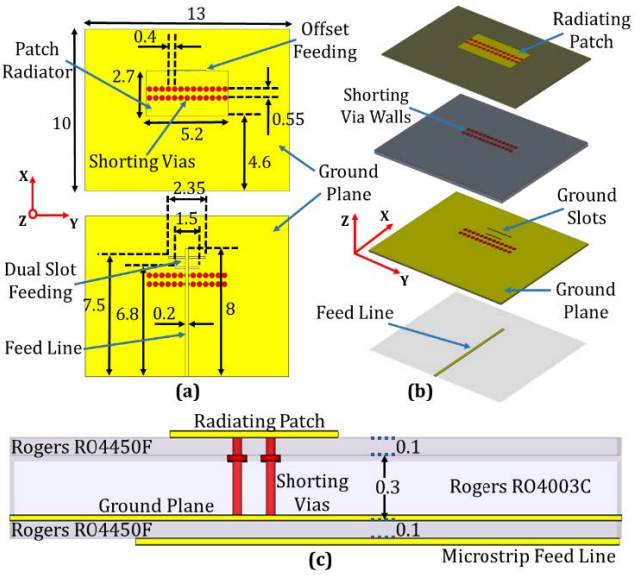

FIGURE 1. Schematics of the proposed shorted patch 5G mmWave AiP design (a) top view, (b) perspective view and (c) side view (All dimensions are in mm).

II. BEAM-TILTED, SINGLE-PATCH AiP DESIGN

Fig. 1 depicts the configuration of the dual-aperture-based, 5G mmWave AiP design. The design is compact in size with the overall dimensions 0.5 mm × 10 mm × 13 mm. The antenna is fabricated on the Rogers RO4003C (core layer) and Rogers RO4450F (prepeg layers) substrate stack-up respectively with loss tangent of 0.0027 and 0.004 and dielectric constant of 3.55 ± 0.05 and 3.52 ± 0.05. This multilayered substrate in this paper is cheaper and provides an ease of fabrication compared with the LTCC substrate. For the multilayered antenna fabrication, the industry standard is to use one core layer followed by a prepeg layer. In the proposed antenna topology, the core Rogers RO4003C layer is sandwiched between two prepeg Rogers RO4450F layers. The prepeg layer is thinner than core layer that is primarily used for binding and insulation purposes. In addition, the dielectric properties of the core and prepeg layers does not vary to a large extent with each other. Furthermore, the proposed AiP design consists of three substrate layers with a total thickness of 0.5 mm (~0.05-λ_0 at 28 GHz), which is very thin in comparison with other reported 5G mmWave AiPs in the literature [9], [10], [11].

The top layer has a rectangular patch radiator with a length of 2.7 mm, corresponding to a half-wavelength at 29.5 GHz. The aperture-coupled feeding is used with a 50Ω microstrip feed line to excite the patch through the two slots in the ground plane. The aperture-coupled feeding helps in the reduction of cross-polarization and spurious radiation from the microstrip feed line. Two shorting via walls are introduced in the middle of patch to excite the $TM^z_{1/2,0,0}$ mode at lower frequencies and to divert the radiation beam from

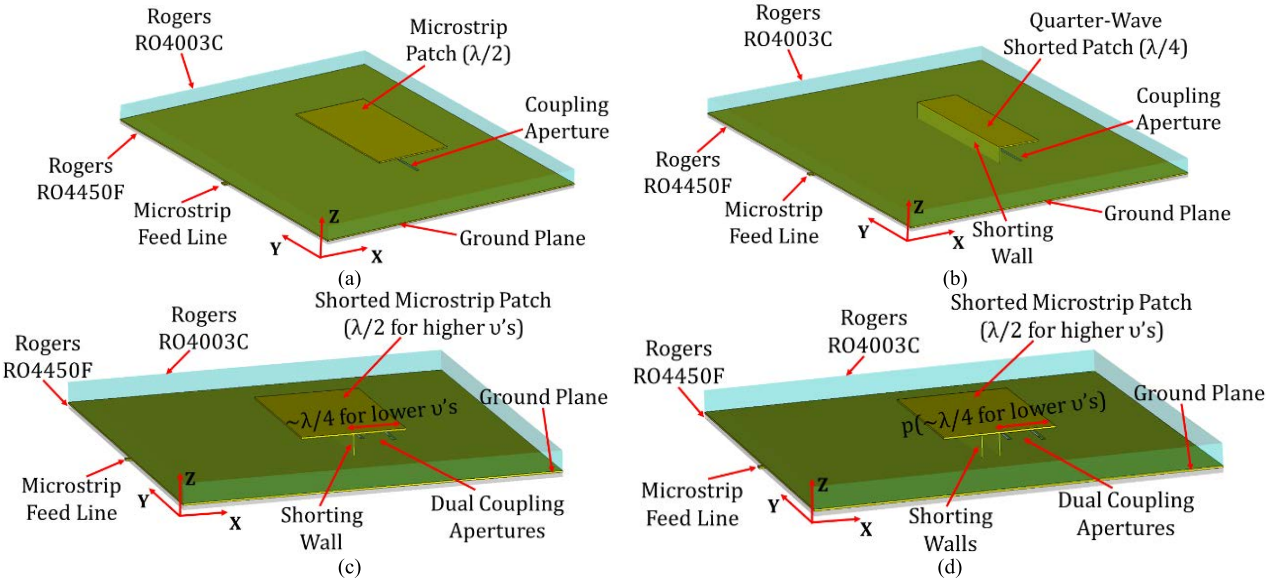

FIGURE 2. Evolution of the proposed single-patch design. (a) Conventional microstrip patch antenna (MPA). (b) Quarter-wavelength shorted patch antenna (QW-SPA). (c) Extended SPA with two slots in the ground. (d) Proposed design with two shorting via walls.

the broadside to end-fire direction. To increase the antenna bandwidth for covering the entire n257 frequency band, the patch is extended so that additional mode, $TM^{z}_{1,0,0}$, at higher frequencies can be excited, together with the two slots in the ground plan for increasing coupling.

The multiple shorting vias inserted in the patch antenna have a diameter of 0.2 mm and a pad diameter of 0.33 mm with the distance of 0.4 mm between each via. The apertures in the ground plane are offset from the center of rectangular patch, and the shift of 0.4 mm is introduced from the edge of via wall. This is primarily done to enhance the coupling to one end of the patch (opposite to feeding side) so that the beam tilt can be significant enough at higher frequencies.

The RF circuitry can also influence the impedance of the microstrip feed line, which can be prevented by using another ground layer below the feed line. However, the feed line needs to be redesigned as 50 Ω stripline rather than 50 Ω microstrip feed line. In this work, a full-metal ground layer is used for shielding the proposed design from other RF circuitry underneath the patch.

A. EVOLUTION AND WORKING PRINCIPLE OF THE SINGLE-PATCH AiP DESIGN

This section describes the evolution and the working principle of the proposed single-patch AiP design. Firstly, a conventional, microstrip patch antenna (MPA) is designed and excited by the aperture-coupled feeding as shown in Fig. 2(a). The resonant length of the patch corresponds to a half-wavelength at 28 GHz. As per the cavity model [13], the electric field within the cavity of the MPA in Fig. 2(a) can be expressed as:

$$\vec{E} = \hat{z}E_z \tag{1}$$

For this antenna, the narrow impedance bandwidth of less than 5% is only obtained. The dominant $TM^{z}_{1,0,0}$ mode is excited with the radiation beam normal to the patch radiator. The resonant frequency corresponding to the fundamental mode of the MPA is equal to:

$$(f_r)_{1,0,0} = \frac{c}{2\pi\sqrt{\varepsilon_r}}\frac{\pi}{a} = \frac{c}{2a\sqrt{\varepsilon_r}}, \tag{2}$$

where 'c' is the speed of light in free space, 'a' denotes length of the radiator, and 'ε_r' is the relative permittivity of dielectric substrate.

To achieve the beam tilt toward the end-fire direction, a quarter-wavelength shorted patch antenna (QW-SPA) is next designed as shown in Fig. 2(b). The virtual shorting of the MPA is replaced by the shorting via wall in the QW-SPA. This way, the patch frequencies remain unvaried at 28 GHz. Also, the compactness can be obtained as the patch size decreases. However, the antenna gain is sacrificed, because the size of the QW-SPA is one-half of the conventional MPA.

For the QW-SPA, the dominant $TM^{z}_{1/2,0,0}$ mode corresponds to the lowest order resonance given by:

$$(f_r)_{1/2,0,0} = \frac{c}{2\pi\sqrt{\varepsilon_r}}\frac{\pi}{2a} = \frac{c}{4a\sqrt{\varepsilon_r}} \tag{3}$$

The impedance bandwidth obtained for this antenna is still narrow and less than 5%. As illustrated in Fig. 3, the broadside radiation pattern of the MPA shows almost zero beam tilt with the antenna boresight at 0°, whereas the radiation of the QW-SPA has a beam tilt of around 20° in the E-plane. The beam tilt from the QW-SPA can also be validated from various designs [14], [15]. The beam tilt in the E-plane can be attributed to the shorting wall, which acts as a reflector placed a quarter-wavelength away from the radiating edge. Although

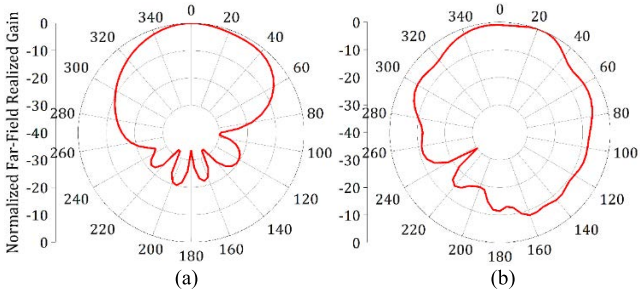

FIGURE 3. Radiation patterns in the E-plane for (a) MPA and (b) QW-SPA.

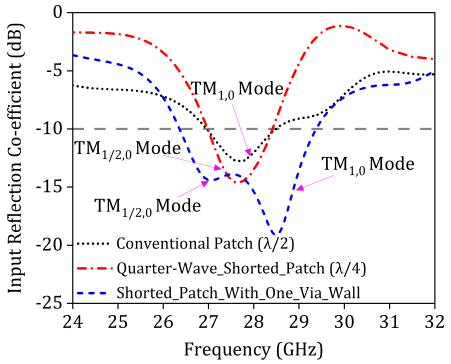

FIGURE 4. Reflection co-efficient for the cases studied of Fig. 2(a), 2(b), and 2(c).

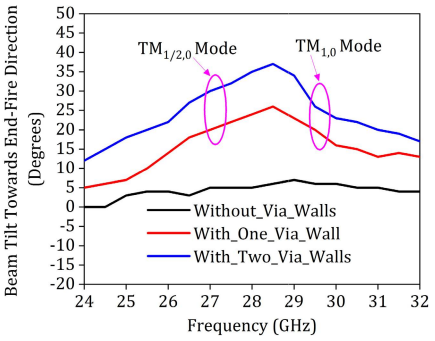

FIGURE 5. FIGURE 5. Comparison of the beam tilt for the cases of Fig. 2(a), (c), and (d).

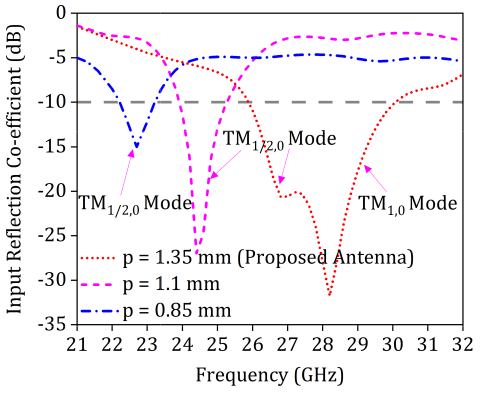

FIGURE 6. Reflection co-efficient for the various location p of the shorting via walls for the proposed design in Fig. 2(d).

the QW-SPA retains the advantages of the size reduction and the beam tilt, it suffers from higher cross-polarization [16].

The impedance bandwidth of the MPA and QW-SPA is limited and cannot meet the n257 frequency band. To increase the bandwidth, various bandwidth enhancement techniques have been proposed for the QW-SPAs, for example, cutting a U-shaped slot in the patch [14] or adding the shorting pins and V-shaped slots in the patch [17]. These techniques cannot be implemented for the proposed design, in which the end-fire radiation beam is demanded. Also, these antennas suffer from high cross-polarization in the H-plane. Therefore, for bandwidth enhancement, the patch is extended in such a way that additional mode, $TM^z_{1,0,0}$, at higher frequencies can be excited, together with the two slots used in the ground for increasing coupling. This $TM^z_{1,0,0}$ mode corresponds to the entire length of the patch that suggests the two radiating slots would contribute to the radiation normal to the patch. In this case, the beam tilt will be minimal at higher frequencies. To enhance the beam tilt at higher frequencies, the offset of the two slots is further applied in the ground as depicted in Fig. 2(c). It should be further noted that the size of dual apertures present in the ground plane should be kept electrically small for avoiding any spurious radiation from them. Fig. 4 shows the reflection co-efficient for the cases in Fig. 2(a)-(c). It is clearly seen that the MPA and QW-SPA have narrower impedance bandwidth (∼4.7%), while the case in Fig. 2(c) has two excited modes, $TM^z_{1/2,0,0}$ and $TM^z_{1,0,0}$, to cover a wide operating band with the fractional bandwidth of around 10.8%.

The beam tilt produced by the incorporation of the shorting wall and the offset feeding is around 15–25 degrees, which wouldn't be enough, because the end-fire gain will be minimal. To further tilt the beam, the additional shorting wall is added as displayed in Fig. 2(d). The shorting wall act as a second reflector and can enhance the beam tilt around 26–37 degrees. The beam-tilt variation for the cases in Fig. 2(a), (c), and (d) is illustrated in Fig. 5. Beam tilt here indicates as the angle between antenna broadside direction and antenna boresight. In general, the beam tilt is increased as the antenna frequency increases, due to the increase in the electrical size of the reflector (shorting walls). However, the beam tilt is reduced at higher frequencies because of the excited $TM^z_{1,0,0}$ mode. It should be noted here that the beam squint can also be attained by using superstrate layer(s) on the top of antenna as can be observed in [18], [19], and [20]. However, the superstrate layer(s) need to be installed at some distance on the top of primary radiator. This increases the overall size of antenna that limits its usage for modern slim 5G mmWave devices.

The two shorting via walls around the middle of the patch are introduced so as to preserve the odd symmetry for the $TM^z_{1,0,0}$ mode. The placement of the shorting walls influence the excited modes of the proposed patch. The parameter 'p' as shown in Fig. 2(d) is varied, and its influence on the antenna frequencies is illustrated in Fig. 6. The $TM^z_{1,0,0}$ mode

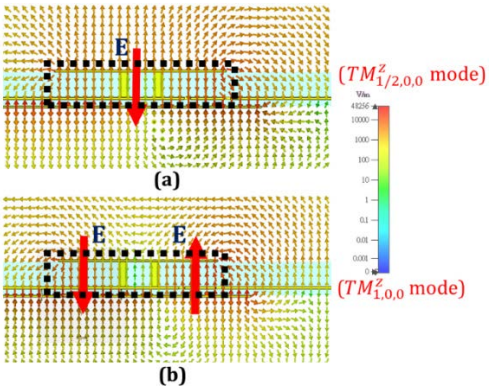

FIGURE 7. Vector electric-field distribution for the proposed single-patch design at (a) 26.5 GHz and (b) 29.5 GHz.

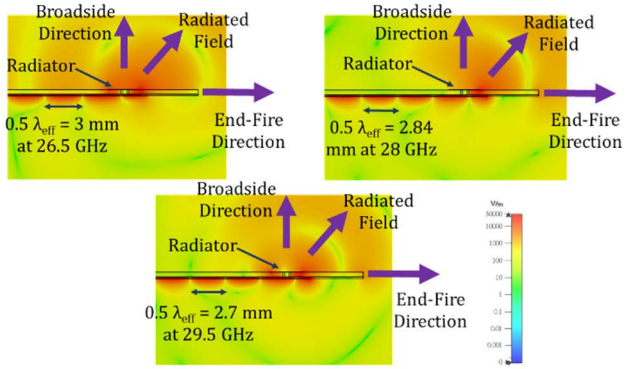

FIGURE 8. Electric fields in the contour plot at 26.5, 28 and 29.5 GHz.

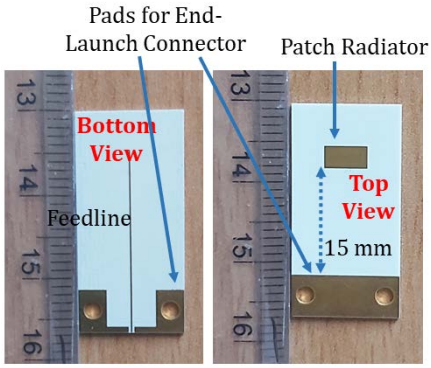

FIGURE 9. Photograph of the fabricated single-patch AiP design.

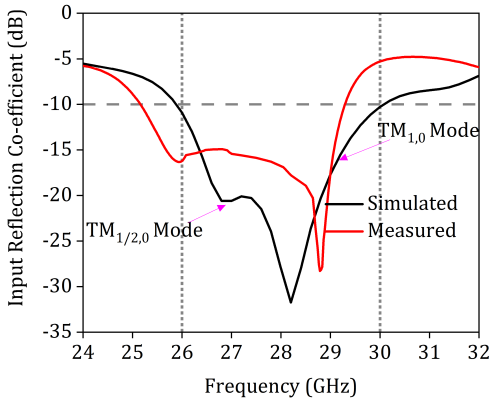

FIGURE 10. Simulated and measured reflection co-efficient of the proposed single-patch AiP design.

disappears when the shorting walls move away from the patch center. This is because the odd antenna symmetry gets deteriorated and the electric field null is changed from the patch center. Also, the length of the QW-SPA is increased, and therefore the resonant frequency of the $TM^z_{1/2,0,0}$ mode decreases.

B. ELECTRIC FIELD DISTRIBUTION

The vector electric-field distribution for the single-patch AiP at lower frequency of 26.5 GHz and higher frequency of 29.5 GHz is presented in Fig. 7. The results in Fig. 7(a) show no variation along the resonant length of the patch. The electric field corresponds to a quarter-wavelength from the radiating edge of the shorted patch. That is, the $TM^z_{1/2,0,0}$ mode is excited at lower frequencies thereby acting as a fundamental mode of the proposed antenna. Note that the subscript ''1/2'' in $TM^z_{1/2,0,0}$ means that the electric field variation is the same as that of the conventional MPA. In Fig. 7(b), the variation in the electric field occurs one time around the shorting via walls. The electric field is odd symmetrical with respect to the shorting via walls of the patch. In this case, the $TM^z_{1,0,0}$ mode is excited at higher frequencies. The corresponding electric fields in the contour plot at 26.5, 28 and 29.5 GHz are illustrated in Fig. 8. It can be observed that the half-wavelength transmission mode demonstrates the beam tilt obtained at these frequencies.

C. SIMULATED AND MEASURED RESULTS

The photo of the fabricated prototype of the proposed single-patch AiP design is shown in Fig. 9. For proper visualization, end-launch connector is not included in the photograph of the fabricated prototype. A separation distance of 15 mm (∼1.5-λ at 28 GHz) is chosen between the end-launch connector and the patch in order to avoid the deterioration in the radiation patterns and the impedance mismatch caused by the connector. Note that through-reflect-line (TRL) calibration technique was used for *S*-parameter measurement [21]. The reference plane can be chosen closer to the patch radiator to match the simulation structure, removing the unwanted effects of the connector and the insertion loss of the feed line.

The simulated and measured reflection co-efficient of the proposed single-patch design is depicted in Fig. 10. The results show a wide operating band, covering the frequencies ranging from 26 to 30 GHz with the fractional bandwidth of around 14.3%. This indicates the single-patch AiP design can cover the 5G mmWave band n257 (26.5–29.5 GHz). Note that there is a frequency shift in the measured reflection co-efficient, which is mainly due to the variation in dielectric constants of the substrate stack-up between the simulation and the fabrication. Moreover, the difference between the simulated and measured results could be caused by the variation of the characteristic impedance of the end-launch connector from 50 Ω [22].

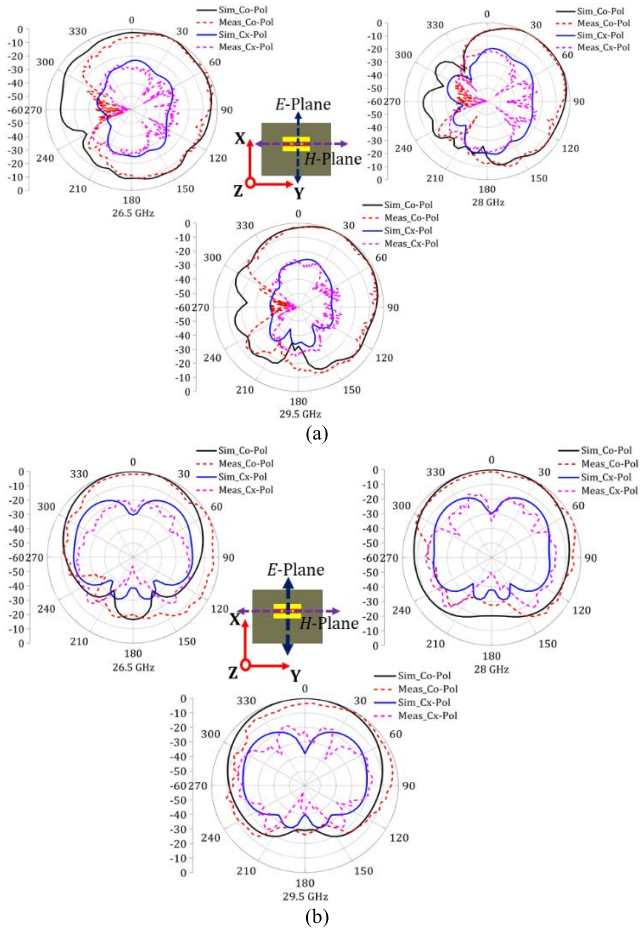

FIGURE 11. Simulated and measured radiation patterns in the (a) E-plane and (b) H-plane.

Fig. 11 shows the co-polarization (co-pol) and the cross-polarization (cross-pol) radiation patterns for the proposed single-patch design in both principal planes, E-plane (x-z plane) and H-plane (y-z plane). It is seen that the beam tilt is obtained in E-plane over the operating band. The beam tilt of around 35 degrees with the gain of around 2.5 dBi toward the end-fire direction is observed at 28 GHz.

The cross-polarization is less than -20 dB in the E-plane but slightly higher in the H-plane. This is because the non-zero E_φ-component in the H-plane as non-radiating slots also contribute to some radiation. However, the cross-pol level is still less than -12 dB, much smaller than other QW-SPAs [23], [24], due to the use of the thin dielectric substrate and the aperture-coupled feeding. The proper adjustments of W/L (here $W = 5.2$ mm and $L = 2.7$ mm) also help reduce cross-polarization [25]. Note that large discrepancies between the simulated and measured back-side radiation are due to the blockage and scattering radiation from the rotating platform and probes in the far-field chamber. On the other hand, good agreement between the simulated and measured results in the other half-space above the patch are obtained.

Fig. 12 shows the simulated and measured peak antenna gain and efficiency. Measured gain is calculated by using

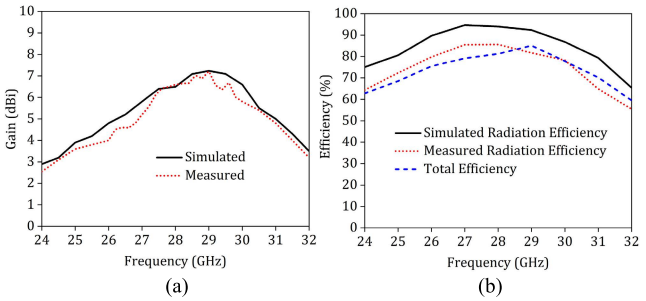

FIGURE 12. (a) Peak antenna gain and (b) efficiency of the proposed single-patch AiP design.

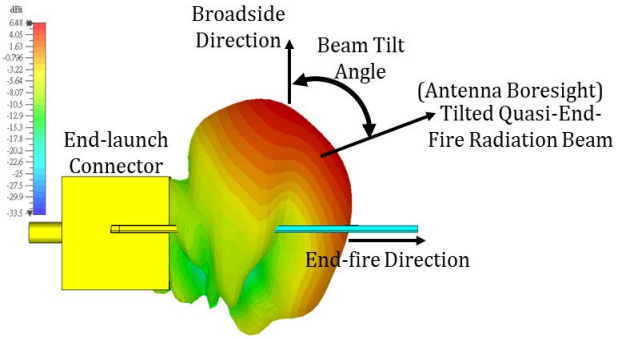

FIGURE 13. 3-D radiation pattern of the proposed single-patch AiP design at 28 GHz.

the standard gain transfer method [26]. In Fig. 12(a), the peak gain varies from 5 to 7.3 dBi over the operating band. The lower gain at lower frequencies is obtained due to a smaller electrical size ($\lambda/4$) of the patch at those frequencies in contrast to the larger size ($\lambda/2$) of the patch at higher frequencies. The radiation and total efficiency of the proposed single patch is shown in Fig. 12(b). Good radiation efficiency more than 87% is observed over the entire operating band. Finally, Fig. 13 plots the 3-D radiation pattern at 28 GHz for the proposed single-patch AiP design. It can be easily seen in the figure that the tilted beam radiation is toward the end-fire direction.

III. DIFFERENTIAL-FED, SUB-ARRAY AiP DESIGN

To achieve more beam tilt toward the end-fire direction, the differential-fed, two-patch sub-array formed by two single-patch design studied in the previous section is proposed here. Fig. 14 illustrates the schematics of the proposed AiP design. The proposed two-patch sub-array AiP possesses the overall dimensions of 0.5 mm $\times$ 18 mm $\times$ 20 mm. The substrate size is chosen large enough for accommodating the end-launch connector. The height of the design is kept the same as 0.5 mm as shown in Fig. 1. The two patch antennas are spaced apart by a half-wavelength ($0.5\lambda_0$) at 28 GHz. This spacing is significant enough to produce low mutual coupling. For the proposed sub-array antenna geometry, isolation between the proposed QW-SPA elements is greater than 16 dB over the band, which signifies minimal power loss. The single QW-SPA is expanded into the

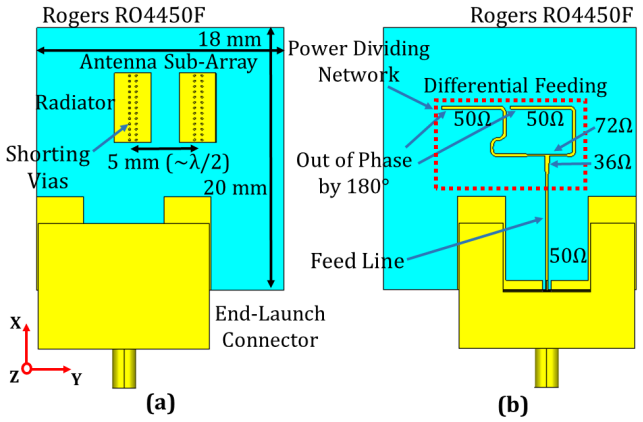

FIGURE 14. Schematics of the proposed, differential-fed, sub-array AiP design. (a) Top view and (b) bottom view.

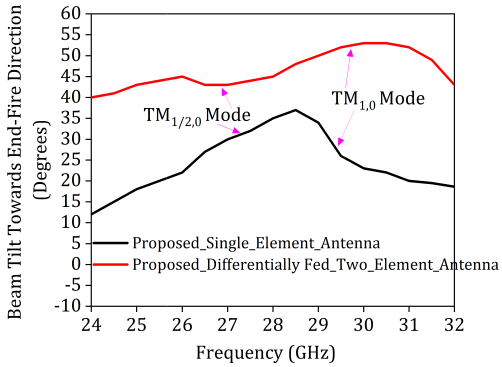

FIGURE 15. Comparison of the beam tilt between the single-patch and the sub-array AiP designs.

differential-fed two-patch sub-array for achieving the quasi-end-fire AiP design. The differential feeding is used, in which a 180-degree phase difference is realized by a microstrip-feed-line-based 1:2 power divider. A delay line is used for creating a 180-degree phase difference between the feed lines. The two patch radiators are aligned in series along the resonant length of the patch in order to obtain larger beam tilt toward the end-fire direction. A GCPW-microstrip transition is used for the practical antenna topology when the design is mounted with end-launch connector.

The enhancement of the beam tilt between the single-patch and the sub-array AiP designs is depicted in Fig. 15. For the sub-array AiP design, the beam tilt varies from 43–53 degrees over the entire operating band. Compared with the single-patch design in Fig. 1, the beam tilt for the sub-array is increased by around 17 degrees. Note at higher frequencies, the beam tilt is increased more, which could be attributed to the array effect.

A. ELECTRIC FIELD DISTRIBUTION

The excited resonant modes in the proposed sub-array design are the same as those studied in Fig. 7 for the single-patch design. The $TM^z_{1/2,0,0}$ and $TM^z_{1,0,0}$ modes resonate at lower and higher frequencies respectively. The distribution of the vector electric fields in the cross section along the resonant

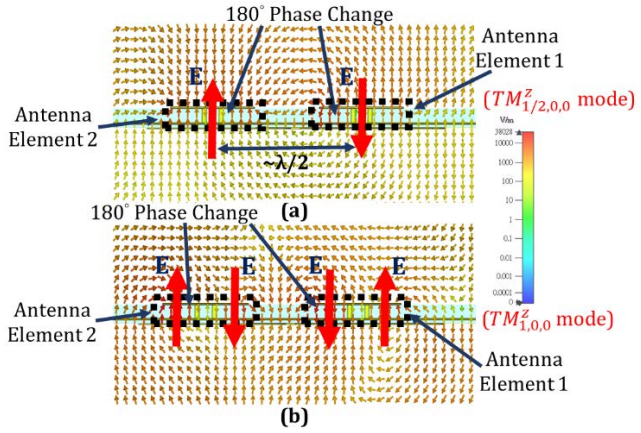

FIGURE 16. Vector electric-field distribution for the proposed sub-array design at (a) 26.5 GHz and (b) 29.5 GHz.

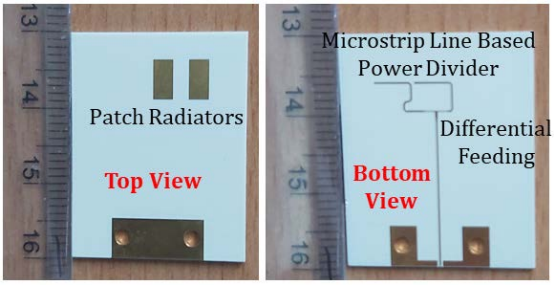

FIGURE 17. Photograph of the fabricated sub-array array AiP design.

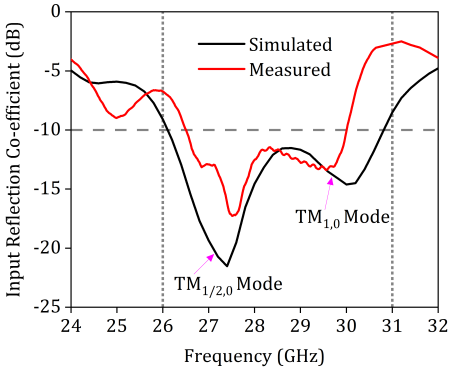

FIGURE 18. Simulated and measured reflection co-efficient of the proposed sub-array AiP design.

length of the patches are illustrated in Fig. 16. The phase reversal can be clearly seen between the two patch radiators that are simultaneously excited.

B. SIMULATED AND MEASURED RESULTS

The fabricated prototype of the differential-fed, sub-array AiP design is shown in Fig. 17. The simulated and measured reflection co-efficient of the proposed sub-array design is depicted in Fig. 18. A wide operating band with a 4.7 GHz bandwidth that corresponds to around a 16.5% fractional bandwidth can be achieved. As discussed in the previous section, the discrepancies between the simulated and measured results are attributed to the dielectric-constant variation

TABLE 1. Comparison of the proposed 5G mmWave AiP design with other recently reported antennas.

Parameters	[5]	[9]	[10]	[11]	[28]	[29]	Proposed Work
Antenna Type	PFSA	Dual Dipole	SIW horn	Electric Dipole	Folded Dipole + Bridge Antenna	SIW	**Shorted Patch**
Frequency Band (GHz) (FBW)	36.24 – 40 (9.8%)	28.4 – 30.1* (5.1%)	27.5 – 29* (5.3%)	24.3 – 31.53 (12.9%)	25.4 – 30.8* (19.2%) 38 – 40*(5.1%)	36 – 40 (10.5%)	**26.4 – 29.8 (12.1%)**
Thickness (λ_0)	0.11 at 38 GHz	0.12 at 28 GHz	0.11 at 28 GHz	0.49 at 28 GHz	0.11 at 28 GHz	0.13 at 38 GHz	**0.05 at 28 GHz**
Peak Gain (dBi)*	2.43	4.9	6.75	7.13	7.02	5.2	**8.2**
End-fire Gain (dBi) at center frequency	< 2.3	4.9	6.75	7.13	5.59 (at 28 GHz) 6.33 (at 39 GHz)	5.2	**6**
Peak Antenna Efficiency (%)	94	90 (H-pol) 80 (V-pol)	Not Available	95	Not Available	Not Available	**80**
3-dB Beamwidth in E-plane (degrees)	190	Not Available	98	135.6	< 70	90 – 100	**82**
Ground Plane Implementation	Full	Partial	Partial	Partial	Partial**	Full	**Full**
Ground Clearance (mm)	0	2.3	2.7	10	1.2	0	**0**
Radiation Pattern Type	Quasi-end-fire	End-fire	End-Fire	End-fire	Quasi-end-fire	End-fire	**Quasi-end-fire**
Cost	High	High	Low	Low	Low	Low	**Low**
Beam Tilt (from the broadside direction)	70° at 39 GHz	0°	0°	0°	50° at 39 GHz	0°	**45° at 28 GHz**

* Measured overlapped impedance bandwidth/peak gain for H-pol and V-pol is used
** A large metallic plate is used underneath the antenna at the distance of 5 mm
PFSA = planar folded slot antenna, SIW = substrate integrated waveguide and FBW = fractional bandwidth

of the substrate, fabrication tolerance, and the solderless contact between the feed line and the end-launch connector.

The simulated and measured radiation patterns for the proposed, differential-fed, sub-array design are presented in Fig. 19. Due to the incorporation of the patch array, the beam tilt is enhanced and reaches around 45 degrees at 28 GHz. In addition, the peak gain of more than 5 dBi toward the end-fire direction is obtained. The cross-polarization is observed less than −20 dB and −15 dB in the E-plane and H-plane respectively. The aperture-coupled feeding and differential feeding [27] also help reduce the cross-polarization in both principal planes, particularly in the H-plane where the cross-polarization is high due to the excited $TM^{z}_{1/2,0,0}$ mode. Similar to the results seen in Fig. 11, the proposed sub-array design suffers from large variation of the back-side radiation between the simulated and measured patterns. Again, this is because the scattering radiation from the rotating platform for the antenna-under-test (AUT) in the chamber.

Fig. 20 shows the simulated and measured peak antenna gain and efficiency. It can be seen in Fig. 20(a) that optimal peak gain of around 8.2 dBi is obtained over the operating band. The radiation and total efficiency of the proposed sub-array is plotted in Fig. 12(b). The radiation efficiency of more than 80% is observed over the entire operating band. Note that the total efficiency is comparatively less than the radiation efficiency as the former includes losses caused by the impedance mismatch at the connector and the dielectric and conductive losses. Fig. 21 shows the corresponding 3-D radiation pattern for the sub-array AiP design. The quasi-end-fire radiation beam can be clearly noted and is directed toward the end-fire direction with high antenna gain.

A comparison table for the proposed sub-array AiP design and other reference works are also provided in this section. Table 1 compares the performance and characteristics of the proposed sub-array with some recent 5G mmWave antenna designs. The proposed design possesses a very low thickness in comparison with other designs. It can be also noted that the proposed antenna acquires a wide impedance bandwidth with high optimal gain of 8.2 dBi. The proposed design also uses the full-metal ground for better shielding of the radiator

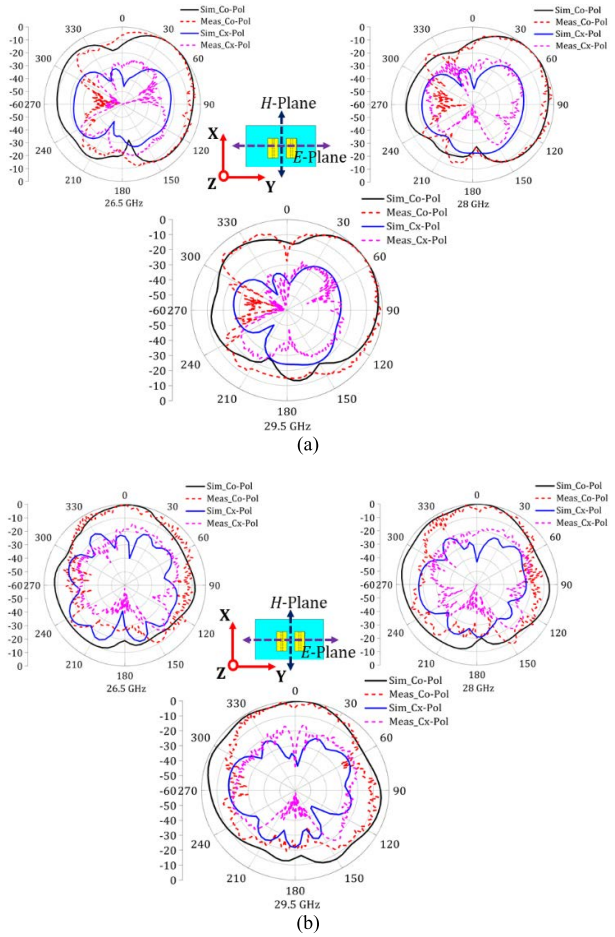

FIGURE 19. Simulated and measured radiation patterns in the (a) E-plane and (b) H-plane.

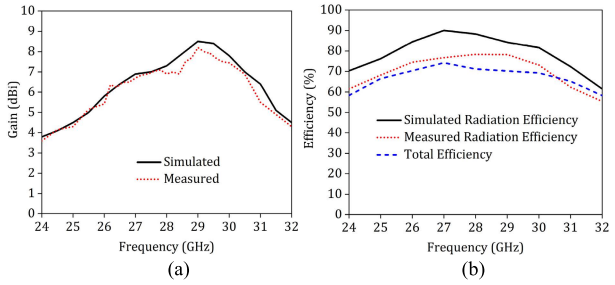

FIGURE 20. (a) Peak antenna gain and (b) efficiency of the proposed sub-array AiP design.

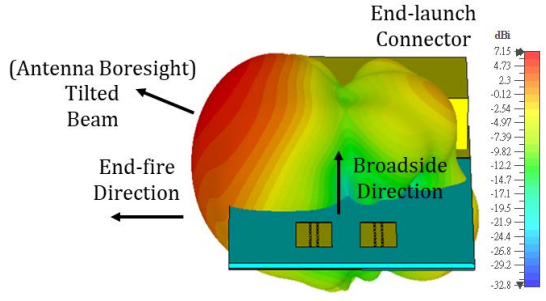

FIGURE 21. 3-D radiation pattern of the proposed sub-array AiP design at 28 GHz.

from the RF circuitry underneath the patch, which makes it suitable for commercial 5G mmWave mobile applications.

IV. CONCLUSION

A thin, differential-fed two-patch sub-array AiP design for 5G mmWave mobile applications been presented and tested. The proposed AiP design consists of the two dual-aperture-coupled shorted patches differentially fed by a pair of out-of-phase feed line and shows an overall thickness of 0.5 mm (0.05-λ_0 at 28 GHz) only. The proposed design has wide-band performance due to the excitation of the $TM^z_{1/2,0,0}$ and $TM^z_{1,0,0}$ modes that aid in the entire coverage of the n257 frequency band. The obtained fractional bandwidth is around 14.3%, and the beam tilt at 28 GHz is around 45 degrees toward the end-fire direction. In addition, the quasi-end-fire gain of more than 5 dBi is also achieved. Finally, because of the inclusion of the full-metal ground/shielding plane, the proposed AiP design can be easily integrated into the modern 5G mmWave devices.

REFERENCES

[1] C.-X. Wang, F. Haider, X. Gao, X.-H. You, Y. Yang, D. Yuan, H. M. Aggoune, H. Haas, S. Fletcher, and E. Hepsaydir, "Cellular architecture and key technologies for 5G wireless communication networks," *IEEE Commun. Mag.*, vol. 52, no. 2, pp. 122–130, Feb. 2014.

[2] J. Seo, I. Yoon, J. Jung, J. Ryoo, J. Park, W. Lee, D. Ko, and J. Oh, "Miniaturized dual-band broadside/endfire antenna-in-package for 5G smartphone," *IEEE Trans. Antennas Propag.*, vol. 69, no. 12, pp. 8100–8114, Dec. 2021.

[3] S. Liao and Q. Xue, "Dual polarized planar aperture antenna on LTCC for 60-GHz antenna-in-package applications," *IEEE Trans. Antennas Propag.*, vol. 65, no. 1, pp. 63–70, Jan. 2017.

[4] A. Townley, P. Swirhun, D. Titz, A. Bisognin, F. Gianesello, R. Pilard, C. Luxey, and A. M. Niknejad, "A 94-GHz 4TX-4RX phased-array FMCW radar transceiver with antenna-in-package," *IEEE J. Solid-State Circuits*, vol. 52, no. 5, pp. 1245–1259, May 2017.

[5] J. Park, H. Seong, Y. N. Whang, and W. Hong, "Energy-efficient 5G phased arrays incorporating vertically polarized endfire planar folded slot antenna for mmWave mobile terminals," *IEEE Trans. Antennas Propag.*, vol. 68, no. 1, pp. 230–241, Jan. 2020.

[6] Z. Yue, Y. Liu, C. Zhao, A. Ren, Y. Chen, Y. Jia, Y. Xu, and M. Ye, "A dual-polarized end-fire mmWave antenna array without ground clearance for 5G mobile terminals," *Int. J. RF Microw. Comput.-Aided Eng.*, vol. 31, no. 5, May 2021, Art. no. e22576.

[7] J. Park, S. Y. Lee, and W. Hong, "Wideband 39 GHz vertically-polarized endfire antenna-in-package (AiP) array featuring near-planar profile," in *Proc. Int. Symp. Antennas Propag. (ISAP)*, Busan, South Korea, Oct. 2018, pp. 1–2.

[8] M. I. Magray, M. F. Nakmouche, and J.-H. Tarng, "A thin dual slot based offset-fed beam tilted mmWave 5G AiP design," in *Proc. Int. Symp. Antennas Propag. (ISAP)*, Taipei, Taiwan, Oct. 2021, pp. 1–2.

[9] H.-T. Chou, S.-J. Chou, J. D. S. Deng, C.-H. Chang, and Z.-D. Yan, "LTCC-based antenna-in-package array for 5G user equipment with dual-polarized endfire radiations at millimeter-wave frequencies," *IEEE Trans. Antennas Propag.*, vol. 70, no. 4, pp. 3076–3081, Apr. 2022.

[10] J. Zhang, K. Zhao, L. Wang, S. Zhang, and G. F. Pedersen, "Dual-polarized phased array with end-fire radiation for 5G handset applications," *IEEE Trans. Antennas Propag.*, vol. 68, no. 4, pp. 3277–3282, Apr. 2020.

[11] W. El-Halwagy, R. Mirzavand, J. Melzer, M. Hossain, and P. Mousavi, "Investigation of wideband substrate-integrated vertically-polarized electric dipole antenna and arrays for mm-wave 5G mobile devices," *IEEE Access*, vol. 6, pp. 2145–2157, 2018.

[12] Y. W. Hsu, T. C. Huang, H. S. Lin, and Y. C. Lin, "Dual-polarized quasi Yagi-Uda antennas with endfire radiation for millimeter-wave MIMO terminals," *IEEE Trans. Antennas Propag.*, vol. 65, no. 12, pp. 6282–6289, Dec. 2017.

[13] Y. T. Lo, D. Solomon, and W. Richards, "Theory and experiment on microstrip antennas," *IEEE Trans. Antennas Propag.*, vol. AP-27, no. 2, pp. 137–145, Mar. 1979.

[14] S. H. Sun, K. F. Man, B.-Z. Wang, and T. P. Wong, "An optimized wideband quarter-wave patch antenna design," *IEEE Antennas Wireless Propag. Lett.*, vol. 4, pp. 486–488, 2005.
[15] K. L. Lau, K. C. Kong, and K. M. Luk, "A miniature folded shorted patch antenna for dual-band operation," *IEEE Trans. Antennas Propag.*, vol. 55, no. 8, pp. 2391–2398, Aug. 2007.
[16] Y. X. Guo, A. Shackelford, K. F. Lee, and K. M. Luk, "Broadband quarter-wavelength patch antennas with a U-shaped slot," *Microw. Opt. Technol. Lett.*, vol. 28, no. 5, pp. 328–330, Mar. 2001.
[17] N.-W. Liu, L. Zhu, W.-W. Choi, and X. Zhang, "Wideband shorted patch antenna under radiation of dual-resonant modes," *IEEE Trans. Antennas Propag.*, vol. 65, no. 6, pp. 2789–2796, Jun. 2017.
[18] H. Attia, O. Siddiqui, and O. Ramahi, "Beam tilting of single microstrip antenna using high permittivity superstrate," *Microw. Opt. Technol. Lett.*, vol. 55, no. 7, pp. 1657–1661, Jul. 2013.
[19] Q.-Y. Guo and H. Wong, "Wideband and high-gain Fabry–Pérot cavity antenna with switched beams for millimeter-wave applications," *IEEE Trans. Antennas Propag.*, vol. 67, no. 7, pp. 4339–4347, Jul. 2019.
[20] B. P. Chacko, G. Augustin, and T. A. Denidni, "Tilted-beam superstrate antenna with low-profile and high-gain," in *Proc. IEEE Int. Symp. Antennas Propag. (APSURSI)*, Jun. 2016, pp. 341–342.
[21] T.-H. Lin, A. Eid, J. Hester, B. Tehrani, J. Bito, and M. M. Tentzeris, "Novel additively manufactured packaging approaches for 5G/mm-wave wireless modules," in *Proc. IEEE 69th Electron. Compon. Technol. Conf. (ECTC)*, Las Vegas, NV, USA, May 2019, pp. 896–902.
[22] M. I. Magray, G. S. Karthikeya, K. Muzaffar, S. K. Koul, and A. H. Moon, "Wideband asymmetric coplanar strip fed antennas with pattern diversity for mmWave 5G base stations," *IEEE Access*, vol. 8, pp. 77482–77489, 2020.
[23] N.-W. Liu, L. Zhu, and W.-W. Choi, "A low-profile wide-bandwidth planar inverted-F antenna under dual resonances: Principle and design approach," *IEEE Trans. Antennas Propag.*, vol. 65, no. 10, pp. 5019–5025, Oct. 2017.
[24] C. Y. Chiu, K. M. Shum, C. H. Chan, and K. M. Luk, "Bandwidth enhancement technique for quarter-wave patch antennas," *IEEE Antennas Wireless Propag. Lett.*, vol. 2, pp. 130–132, 2003.
[25] R. Garg, P. Bhartia, I. Bahl, and A. Ittipiboon, *Microstrip Antenna Design Handbook*. Boston, MA, USA: Artech House, 2001.
[26] R. A. Alhalabi and G. M. Rebeiz, "Differentially-fed millimeter-wave yagi-uda antennas with folded dipole feed," *IEEE Trans. Antennas Propag.*, vol. 58, no. 3, pp. 966–969, Mar. 2010.
[27] B. Feng, T. Luo, T. Zhou, and C. Sim, "A dual-polarized antenna with low cross polarization, high gain, and isolation for the fifth-generation array/multiple-input multiple-output communications," *Int. J. RF Microw. Comput.-Aided Eng.*, vol. 31, no. 2, Feb. 2021, Art. no. e22278.
[28] M. Rao and K. Sarabandi, "A low-profile dual-band dual-polarized quasi-endfire phased array for mmWave 5G smartphones," *IEEE Access*, vol. 10, pp. 38523–38533, 2022.
[29] J. Zhang, M. O. Akinsolu, B. Liu, and S. Zhang, "Design of zero clearance SIW endfire antenna array using machine learning-assisted optimization," *IEEE Trans. Antennas Propag.*, vol. 70, no. 5, pp. 3858–3863, May 2022.

M. IDREES MAGRAY (Student Member, IEEE) received the B.Tech. degree in electronics and communication engineering from the Islamic University of Science and Technology (IUST), Awantipora, in 2018, and the master's degree from the National Yang Ming Chiao Tung University (NYCU), Taiwan, in 2022.

He is currently working with the Antenna Design Department (ADD), Advanced EM and Wireless Communication Research and Development Center, ASUSTek Computer Inc., Taipei, Taiwan, where he is focusing on the design of Wi-Fi 6E antennas for notebook applications and 5G mmWave antennas in general. He received an INAE Fellowship for two months and during that tenure, he worked under the supervision of Prof. S. K. Koul. He worked on various projects at CARE, IIT Delhi, under the guidance of Prof. S. K. Koul. He has authored and coauthored several papers in peer-reviewed journals and conference proceedings. His research interests include antenna design for notebook applications, co-designed 4G/5G antennas for smartphones, 5G mmWave antennas for mobile terminals and base stations, and antenna-in-packaging (AiP). He received the Best Project Competition Award in IEEE InCAP 2019 and the EECS International Graduate Program Research Award by NYCU, in 2021.

SAOU-WEN SU (Senior Member, IEEE) received the B.S., M.S., and Ph.D. degrees in electrical engineering from the National Sun Yat-sen University, Kaohsiung, Taiwan, in 2001, 2003, and 2006, respectively.

From April 2006 to March 2008, he was with the Technology Research and Development Center, Lite-On Technology Corporation, Taipei, Taiwan, where he was with the Network Access Strategic Business Unit, from April 2008 to February 2012. He built up the first Antenna Design Team at the corporate of the Lite-On Technology Corporation, where he contributed numerous cutting-edge designs to the company's ODM projects, including enterprise and SMB access points, router, Bluetooth headset, home entertainment device, media box, and RF module. Since February 2012, he has been with the ASUSTek Computer Inc., Taipei, where he is currently the Director of the Antenna Design Department, Advanced EM and Wireless Communication Research and Development Center for laptop, 2-in-1 PC, and smartwatch antenna design projects, including ZenBook, VivoBook, StudioBook, ZenWatch, VivoWatch, and ZenFone 2. He has authored 145 refereed papers in international journals and conference proceedings, among which 24 papers are single-author papers conducted on his own. He holds 57 U.S. and 75 Taiwan patents granted, with many patents pending. His published articles have been cited over 3641 times with an H-index of 28 in Google Scholar. He is listed in the *Who's Who in the World 2014*.

Dr. Su is a Senior Member of the IEEE Antennas and Propagation Society and a Life Member of the Institute of Antenna Engineers of Taiwan. He served on the judge panel for the 2014 and 2016 National Terminal Antenna Design Competition organized by the Taiwan Ministry of Economics. He received the one-year full-time School Study Exchange Program Scholarship to The University of Auckland, New Zealand, from the Asian 2000 Foundation, in 1998. He received the Outstanding Technical Achievement Award from the IEEE Tainan Section, in 2016. He served or currently serves as a Reviewer for the IEEE TRANSACTIONS ON ANTENNAS AND PROPAGATION, the IEEE ANTENNAS AND WIRELESS PROPAGATION LETTERS, the *Electronic Letters*, the *IET Microwave, Antennas and Propagation*, and the *Progress in Electromagnetic Research* journals.

JENN-HWAN TARNG (Senior Member, IEEE) received the B.S. degree in power mechanical engineering from the National Tsing Hua University, Hsinchu, Taiwan, in 1981, and the M.S. and Ph.D. degrees in electrical engineering from Pennsylvania State University, University Park, USA, in 1988 and 1989, respectively. He was on leave to the Industrial Technology Research Institute (ITRI) (the largest government founded research), as the General Director of ISTC, from 2007 to 2011, and Service Systems Technology Center (merging two other centers), from 2011 to 2016. He is currently the Co-PI of the Center for mmWave Smart Radar Systems and Technologies (a flag-ship project). In the center, he is also the PI of the sub-project entitled Large and Scalable mmWave Digital Phased Antenna Array. He is also a Professor with the Department of Electrical Engineering and the Dean of the College of Electrical and Computer Engineering, National Yang Ming Chiao Tung University. He has published more than 100 refereed journal articles and conference papers. His research interests include in antennas, RFIC design, radio channel modeling and measurement, and RFID/the Internet of Things (IoT).